Correction for Vascular Artifacts in Cerebral Blood Flow Values Measured by Using Arterial Spin Tagging Techniques

Frank Q. Ye, Venkata S. Mattay, Peter Jezzard, Joseph A. Frank, Daniel R. Weinberger, Alan C. McLaughlin

"Vascular" artifacts can have substantial effects on human cerebral blood flow values calculated by using arterial spin tagging approaches. One vascular artifact arises from the contribution of "tagged" arterial water spins to the observed change in brain water MR signal. This artifact can be reduced if large bipolar gradients are used to "crush" the MR signal from moving arterial water spins. A second vascular artifact arises from relaxation of "tagged" arterial blood during transit from the tagging plane to the capillary exchange site in the imaging slice. This artifact can be corrected if the arterial transit times are measured by using "dynamic" spin tagging approaches. The mean transit time from the tagging plane to capillary exchange sites in a gray matter region of interest was calculated to be ~0.94 s. Cerebral blood flow values calculated for seven normal volunteers agree reasonably well with values calculated by using radioactive tracer approaches.
Key words: cerebral blood flow; perfusion; human; magnetic resonance imaging (MRI).

INTRODUCTION

Steady-state arterial spin tagging approaches have been used to image cerebral blood flow, Q, in animals (1–5) and humans (6–8) by using the equation

$$\Delta M/M_{ss} = -\frac{2 \alpha Q/\lambda}{1/T_1} \qquad [1]$$

where ΔM is the change in brain intracellular water magnetization when arterial spins are perturbed, M_{ss} is the steady-state brain intracellular water magnetization observed during arterial spin tagging, α is the degree of arterial spin inversion, λ is the brain/blood partition coefficient for water, and $1/T_1$ is the observed longitudinal relaxation rate of brain water spins.

One disadvantage of arterial spin tagging approaches is that the small changes in magnetization observed with humans at 1.5 T, e.g., ~2% (6–8), make the approach very sensitive to experimental instabilities and head motion. The sensitivity to experimental instabilities can be minimized by using single-shot imaging techniques, and

recent studies demonstrated that single-shot echo planar imaging (EPI) can be used to obtain reproducible perfusion images of the human head (8).

Another disadvantage of arterial spin tagging approaches is the presence of "vascular" artifacts, which complicate the quantitation of cerebral blood flow values calculated by using Eq. [1]. One vascular artifact observed in human perfusion images is the presence of bright "foci" that are apparently associated with inflow of tagged arterial blood into large arteries (6–8). Although a recent study employed "crusher" gradients to reduce the signal from moving vascular water spins (8), the gradients did not eliminate signals from tagged water spins in large arteries, and no systematic study was performed to determine whether the gradients completely eliminated signals from tagged water spins in small arteries. A significant contribution to $\Delta M/M_o$ from tagged water spins in small arteries could cause a substantial overestimate of cerebral blood flow by using Eq. [1].

A second vascular artifact concerns longitudinal relaxation of tagged arterial blood during transit from the "tagging" plane to capillary exchange sites in the imaging slice. This relaxation reduces α by a factor $\exp(-\tau_a/T_{1a})$, where τ_a is the time required for tagged blood to move from the tagging plane to capillary exchange sites in the imaging slice, and T_{1a} is the longitudinal relaxation time of arterial water spins. Correction for longitudinal relaxation during arterial transit in humans has been difficult because direct estimates of τ_a have not been available.

Arterial spin tagging studies with humans at 1.5 T (6–8) have reported cerebral blood flow values in reasonable agreement with values reported by classical radioactive tracer approaches. However, the effects of the two vascular artifacts discussed above could approximately cancel each other, and the apparent agreement could hide large systematic errors in the spin tagging approach. The work presented here examines both types of vascular artifacts in detail and explores approaches that might be useful in circumventing or correcting for both artifacts.

MATERIALS AND METHODS

Experimental Protocol

Experiments were performed on seven normal subjects by using a protocol approved by the Institutional Review Board of the National Institute of Mental Health.

Twenty-three sagittal images covering the entire head were acquired to localize the slice used for perfusion imaging (see Fig. 1). An axial slice 1–2 cm above the corpus callosum was chosen, and spin echo (SE) images

of this slice were acquired. Spin-echo echo-planar imaging (EPI) approaches were then used to obtain images of this slice in the presence and absence of arterial spin tagging by using a series of values for the amplitude of the bipolar crusher gradients and a series of values for the duration of the off-resonance RF irradiation.

MR Imaging

All imaging experiments were performed on a 1.5 T Signa (General Electric, Milwaukee, WI) scanner employing a 3-axis local gradient head coil (Medical Advances, Milwaukee, WI). The rise time for the gradients was 200 μs and the maximum gradient strength was 2 Gauss/cm.

Anatomical images were acquired using a spin echo sequence with a 256 $\times$ 256 matrix and a slice thickness of 5 mm, with TE = 20 ms and TR = 500 ms.

Spin echo EPI images were obtained using a 64 $\times$ 64 matrix, a 24 cm field of view, a slice thickness of 5 mm, and a TE of 60 ms. Symmetrical gradients were placed immediately before and after the 180° pulse to dephase transverse magnetization excited by the pulse: the width of each pulse was 0.6 ms, and the amplitude of each pulse was 1.7 Gauss/cm. The length of the selective 180° pulse was 3.2 ms. In addition, a pair of bipolar gradients was placed between the 90° and 180° pulses to "crush" the signal from arterial water spins: the width of each pulse was 6 ms, and the separation between the pulses was 2 ms. Bipolar gradients, rather than Stejskal-Tanner gradients, were used in order to minimize TE. The length and separation of the bipolar gradients were chosen to crush adequately the arterial blood signal, while minimizing non-specific effects due to gross motion.

The "nominal" resolution of the 64 $\times$ 64 EPI images, i.e., the resolution calculated ignoring relaxation effects on the point-spread function, was 3.75 mm. Data analysis was performed on images having this nominal resolution. However, for visual presentation EPI images were first "magnified" from 64 $\times$ 64 to 256 $\times$ 256 using 16 identical voxels to represent each original voxel, and then spatially smoothed using "boxcar" averaging. The 16 $\times$ 16 boxcar had weighting coefficients derived from a Gaussian kernal with full-width at half-height of 3.75 mm. The nominal spatial resolution of the resulting image, calculated from computer simulation of the point-spread function, was 5.2 mm.

Spin Tagging

Flow induced adiabatic inversion (2, 9) was used to invert arterial water spins flowing through the "tagging" plane, which was placed 3 cm below the center of the imaging slice (see Fig. 1). Inversion was accomplished by using an off-resonance RF pulse train in the presence of a z gradient. The pulse train consisted of rectangular RF pulses of 75 ms duration separated by 10 ms. The amplitude of the off-resonance RF irradiation (γB_1) was 230 Hz. This value of γB_1 was chosen because previous studies suggested that it produced maximum inversion of arterial water spins at the tagging plane under our conditions (8). The value of α for arterial blood in the tagging plane, α_0, was assumed to be equal to the duty cycle of the RF pulse train (6), i.e., 0.88. The frequency offset of the off-reso-
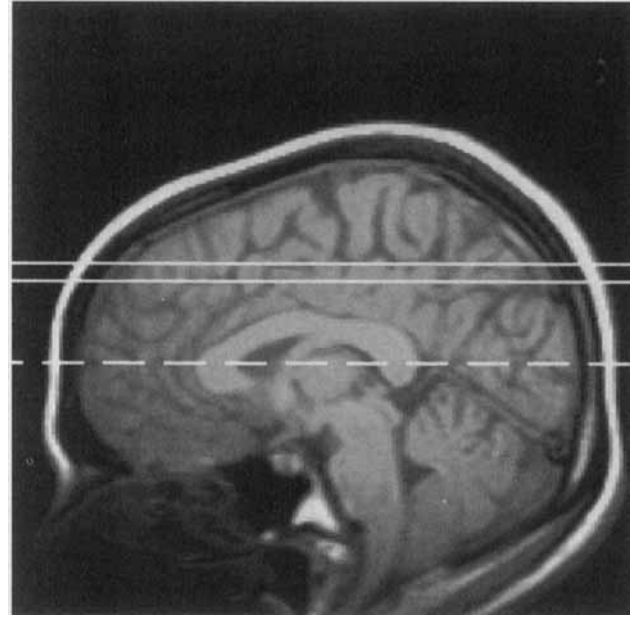

FIG. 1. Sagittal image of a human head showing the location of the imaging slice (solid lines) and the inversion plane (dashed line) used for the perfusion imaging experiments. The position of the slice varied slightly from subject to subject. Distortion of the image at the bottom of the head is due to nonlinearity of the gradient coil in this region.

nance RF irradiation ($\pm$6000 Hz) and the sign of the z gradient ($\pm$200 Hz/mm) were alternated in a four-step protocol to minimize the influence of asymmetric magnetization transfer effects and gradient eddy current effects (5).

Calculation of $R_1(\omega_1,\Delta\omega)$

EPI images were acquired after an off-resonance RF irradiation period of length τ_{RF}. The amplitude of the bipolar crusher gradient was set to zero, and a "fat saturation" pulse, consisting of a 16-ms nonselective sinc pulse followed by gradient spoiler pulses, was added to the sequence.

The z gradient was not turned on during the irradiation. In the absence of a z gradient, the off-resonance RF irradiation did not produce arterial tagging, but did decrease the brain water signal due to magnetization transfer effects. The exponential rate constant for the observed decrease in intensity of the MR signal as a function of τ_{RF} is equal to $R_1(\omega_1,\Delta\omega)$, i.e., the longitudinal relaxation rate in the presence of the off-resonance RF irradiation. Images were acquired with TR = 8 s by using 13 different values of τ_{RF} (0, 0.16, 0.25, 0.33, 0.42, 0.50, 0.67, 0.84, 1.2, 1.5, 1.9, 2.2, and 2.7 s). To obtain adequate precision for the calculated values of M_0 and $R_1(\omega_1,\Delta\omega)$, eight images were acquired with τ_{RF} = 0, while two images were acquired for each of the other τ_{RF} values. $R_1(\omega_1,\Delta\omega)$ and M_0, the equilibrium value of the MR signal in the absence of off-resonance RF irradiation, were calculated from a three-parameter fit to the data (see Fig. 2) by using the "CURFIT" least-squares algorithm (10). The third parameter calculated from the fitting procedure was the steady-
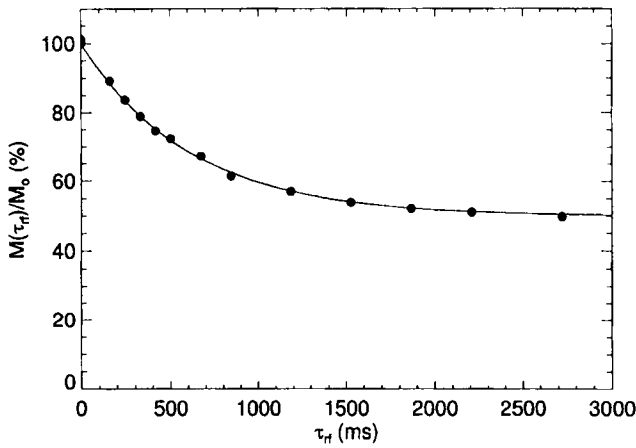
FIG. 2. Dependence of the normalized amplitude of the MR signal from a single gray matter voxel in the imaging slice on the length of the off-resonance RF irradiation, τ_{RF}. ω_1 = 230 Hz, $\Delta\omega$ = 6000 Hz. The fit of the data to a single exponential (solid curve) gives $R_1(\omega_1,\Delta\omega)$ = 1.64 s^{-1}.

state value of the MR signal in the presence of off-resonance RF irradiation.

Dependence of ΔM on the Amplitude of the Bipolar Crusher Gradients

EPI images were acquired with non-zero values of the bipolar crusher gradient, G, by using the four-step protocol for spin tagging (see above). ΔM was calculated for each four-step cycle by subtracting the average image with arterial spin tagging from the average control image

$$\Delta M(\tau_{RF})/M_0 = \qquad\qquad 0 \qquad\qquad 0 \leq \tau_{RF} \leq \tau_a$$

$$= \Delta M(\infty)/M_0 \{1 - \exp[-R_1(\omega_1,\Delta\omega) \quad (\tau_{RF} - \tau_a)]\} \qquad \tau_a < \tau_{RF} \qquad [2]$$

where τ_a is the time required for water to move from the tagging plane to capillary exchange sites in the imaging slice. The signal-to-noise ratio of the $\Delta M/M_0$ values calculated for a single voxel was not sufficient to calculate τ_a for each voxel in the image using Eq. [2]. $\Delta M/M_0$ values for all of the voxels in a gray matter region of interest (ROI) (see below) were thus used to obtain an average value of τ_a for the gray matter ROI.

Determination of τ_a and Q by Using a Modified Protocol

The protocol described above was modified to reduce the total examination time and increase the signal-to-noise ratio of the $\Delta M(\tau_{RF})$ image acquired with τ_{RF} = 3.6 s. ΔM images were obtained in the presence of the large (1.7 Gauss/cm) bipolar crusher gradients by using τ_{RF} = 3.6 s and also seven values of τ_{RF} covering a range from 0.75 to 1.6 s (0.75, 0.83, 1.0, 1.1, 1.3, 1.4, and 1.6 s). Also, one ΔM image was obtained in the absence of the bipolar crusher gradient by using τ_{RF} = 3.6 s. All ΔM images were averaged in an interleaved fashion. ΔM values were normalized by using M_0.

For data acquired in the presence of the large bipolar crusher gradient, a total of 108 four-step cycles were averaged for τ_{RF} = 3.6 s, and a total of 18 four-step cycles were averaged for each of the other τ_{RF} values. For data

(5). Nine ΔM images, each with a different value of G (0, 0.24, 0.48, 0.72, 0.96, 1.2, 1.4, 1.6, and 1.7 Gauss/cm), were acquired in an interleaved fashion. The total length of the off-resonance RF irradiation was 3.6 s, TR = 4 s. The four-step cycle was repeated 36 times for each of the nine ΔM images. The total time for the examination, including a 30-min "set-up" period, was 120 min.

Dependence of ΔM on τ_{RF}

EPI images were acquired after an off-resonance RF irradiation period of length τ_{RF}. Calculated values of ΔM (see above) were normalized by using the equilibrium value of the MR signal, M_0, instead of the steady-state value of the MR signal observed during off-resonance RF irradiation, M_{ss}. The z gradient was on during the irradiation. In the presence of a z gradient, the off-resonance RF irradiation produced both arterial tagging and a decrease in the brain water signal due to magnetization transfer effects. Fifteen values of τ_{RF} were used (0, 0.15, 0.24, 0.41, 0.49, 0.58, 0.75, 0.92, 1.1, 1.3, 1.6, 2.4, 3.0, and 3.6 s). For each value of τ_{RF}, two values of the amplitude of the bipolar crusher gradient, i.e., 0 and 1.7 Gauss/cm, were used. All images were acquired in an interleaved fashion by cycling the values of τ_{RF} and the gradient amplitude, TR = 4 s. Sixteen four-step cycles were averaged to obtain each of the 32 ΔM images. The total time for the examination, including a 30-min "set-up" period, was 160 min.

In the presence of large bipolar gradients that crush the arterial signal, the expected dependence of $\Delta M/M_0$ on τ_{RF} is given by the expression (see Appendix)

acquired in the absence of the bipolar crusher gradient, 18 four-step cycles were averaged. TR = 3.7 s. The total time for the examination, including a 30-min "set-up" period, was 90 min.

Data obtained in the presence of the bipolar crusher gradient were used to calculate the average value of τ_a for the gray matter ROI by using Eq. [2]. Data obtained in the presence of the bipolar crusher gradient with τ_{RF} = 3.6 s were used to calculate Q by using the calculated values of τ_a and $R_1(\omega_1,\Delta\omega)$. Data obtained in the absence of the bipolar crusher gradient, with τ_{RF} = 3.6 s, were used to exclude from the data analysis voxels that had large contributions to $\Delta M/M_0$ due to tagged arterial blood (see below).

Calculation of Cerebral Blood Flow

Cerebral blood flow, Q, was calculated by using the relationship

$$\Delta M(\infty)/M_0 = -\frac{2\,\alpha_{cap}\,Q/\lambda}{R_1(\omega_1,\Delta\omega)} \qquad [3]$$

where $\Delta M(\infty)/M_0$ is the steady-state value of $\Delta M(\tau_{RF})/M_0$, $R_1(\omega_1,\Delta\omega)$ is the longitudinal relaxation rate observed in the presence of off-resonance RF irradiation, and α_{cap} is

the degree of arterial spin inversion at the capillary exchange sites in the imaging slice (11). $\Delta M(\infty)/M_0$ was approximated by $\Delta M(\tau_{RF} = 3.6 \text{ s})/M_0$. Given the range of $R_1(\omega_1, \Delta\omega)$ values in the gray matter ROI and white matter ROI (see below), this assumption should give less than a 3% underestimation in Q. α_{cap} is given by the equation

$$\alpha_{cap} = \alpha_0 \exp(-\tau_d/T_{1a}) \qquad [4]$$

where α_0 is the degree of inversion of arterial water spins at the tagging plane. α_0 was assumed to be 0.88 (see above).

Equation [3] is similar to Eq. [1] but is different in two aspects. First, in Eq. [3] M_0 refers to the equilibrium magnetization observed before application of off-resonance RF irradiation, whereas in Eq. [1] M_{ss} refers to the steady-state magnetization observed in the presence of off-resonance RF irradiation. Second, in Eq. [3] $R_1(\omega_1, \Delta\omega)$ refers to the longitudinal relaxation rate in the presence of off-resonance RF irradiation, whereas in Eq. [1] $1/T_1$ refers to the longitudinal relaxation rate in the absence of off-resonance RF irradiation.

Image Segmentation

EPI images were segmented by using a two-step procedure. The first step used differences in magnetization transfer properties between cerebrospinal fluid (CSF) and brain tissue. In this step, voxels whose steady-state magnetization in the presence of off-resonance RF irradiation was greater than 70% of the equilibrium magnetization were assumed to contain substantial quantities of CSF (12) and excluded. The second step used differences in the observed values of $R_1(\omega_1, \Delta\omega)$ between white and gray matter. In this step, voxels with $R_1(\omega_1, \Delta\omega)$ values between 1.35 and 1.85 s^{-1} were assigned to a gray matter ROI, while voxels with $R_1(\omega_1, \Delta\omega)$ values between 2.27 and 2.94 s^{-1} were assigned to a white matter ROI. These values were chosen so that visual inspection of the resulting segmentation "masks" indicated that voxels in the white matter ROI formed clusters in the location of the white matter tracks, while voxels in the gray matter ROI outlined the cortical strips. The average number of voxels in the gray matter ROI was 280, and the average number of voxels in the white matter ROI was 130. The average number of brain voxels in the image was ~1000.

No attempt was made to assign every brain voxel in the image to gray matter, white matter, or CSF compartments, as has been done in the analysis of high-resolution images (13). However, the simplified procedure outlined here was useful in defining regions that were predominantly gray matter or predominantly white matter, respectively.

Exclusion of "Arterial" Voxels

Images taken in the absence of bipolar crusher gradients were examined, and voxels with $\Delta M/M_0$ values larger than a critical value were assumed to have substantial contributions from arterial blood. These voxels were designated as "arterial" voxels, and excluded from the gray matter ROI and the white matter ROI (see above). The critical value of $\Delta M/M_0$ was chosen so that visual inspection of images taken in the absence of bipolar crusher

gradients showed essentially no bright foci. Critical values of $\Delta M/M_0$ were ~5%. On average, ~7% of the brain voxels in the image were designated as arterial voxels.

Longitudinal Relaxation Time of Oxygenated Blood

Oxygenated human blood was prepared according to the procedure outlined in Brooks *et al.* (14). The hematocrit was 46.2% and the oxygen saturation was 99.9%. The longitudinal relaxation time was measured at 63.9 MHz and $T = 37°C$, according to the procedures outlined in Vymazal *et al.* (15).

RESULTS

Overview of Experimental Protocol

The experiments were divided into two sections. The experiments in the first section studied the dependence of ΔM on the amplitude of the bipolar crusher gradients, and the dependence of ΔM on the length of the off-resonance RF irradiation, τ_{RF}. These experiments were used to design protocols that could be used to minimize vascular artifacts in the cerebral blood flow images. These experiments were performed on a single subject.

The experiments in the second section used a modified protocol that was based on the results obtained in the first section. The modified protocol was designed to allow the calculation of quantitative cerebral blood flow maps in individual subjects. These experiments were performed on seven subjects.

Dependence of ΔM on the Amplitude of the Bipolar Crushers

Figure 3 shows the dependence of ΔM and M_{ss} on the amplitude of the bipolar crusher gradient. At the highest value of the bipolar crusher gradient, "b" (16) was 4.5 s/mm^2 and "V_{enc}" (17) was 1.5 cm/s. In both cases the data were averaged over a gray matter ROI containing
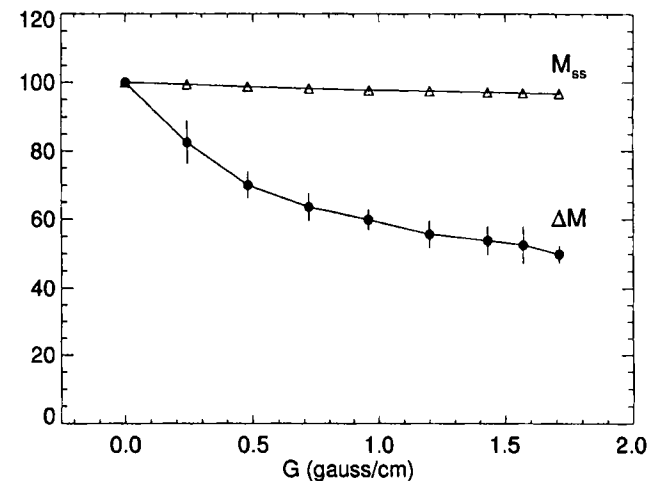

FIG. 3. Dependence of ΔM (filled circles) and M_{ss} (triangles) on the amplitude of the bipolar "crusher" gradient, G. Results were averaged over the gray matter ROI and normalized by using the intial values observed for $G = 0$. Results were also averaged over three separate examinations in the same subject. Data from Subject 4.

approximately 300 voxels (see Materials and Methods). Results are the average of three experiments performed on the same subject (Subject 4) on different days.

Figure 3 demonstrates that increasing the amplitude of the bipolar crusher gradients decreased the value of ΔM by ~49%. However, under the same conditions the control signal, M_{ss}, decreased by only 3%. The decrease in ΔM appeared to plateau at the high gradient amplitudes. Similar results were observed on another subject (Subject 7). The observed plateau suggests that at the high bipolar gradient amplitudes a substantial fraction of the signal from tagged arterial water spins had been "crushed."

Figure 4 shows a series of ΔM images taken at different values of the amplitude of the bipolar crusher gradient.

Dependence of ΔM on τ_{RF}

Figure 5 shows the dependence of ΔM on the length of the off-resonance RF irradiation, τ_{RF}, using two different values for the amplitude of the bipolar crusher gradient, i.e, 0 and 1.7 Gauss/cm. In both cases the data were averaged over a gray matter ROI containing approximately 300 voxels (see Materials and Methods section).

The data obtained in the presence of the strong bipolar crusher gradient can be fit by using Eq. [2], and the average value of $R_1(\omega_1,\Delta\omega)$ for the gray matter ROI, to estimate τ_a. The value of τ_a obtained from the data shown in Fig. 5 was 1.0 s. By using Equation [2] we implicitly assume a single-compartment model for the interpretation of the dependence of $\Delta M(\tau_{RF})$ on τ_{RF}, i.e., that all of the voxels in the ROI have the same value of τ_a. Clearly, this is an approximation, and the calculated value of τ_a must be considered an "average" value. However, the observed fit to the data using Eq. [2] (see solid line in Fig. 5) demonstrates that in the presence of the large bipolar crusher gradient the single-compartment model gives a good description of the data obtained from the gray matter ROI.
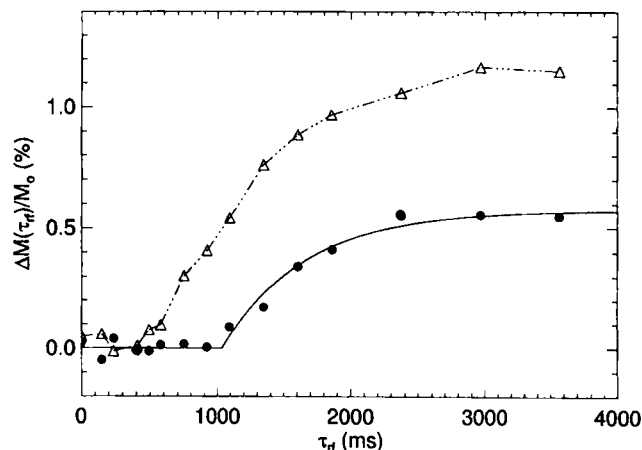

FIG. 5. Dependence of $\Delta M/M_0$ on the length of the off-resonance RF pulse train, τ_{RF}. $\Delta M/M_0$ values were averaged for all voxels in the gray matter ROI. Data were taken in the absence of the bipolar crusher gradient (triangles) and in the presence of a large (1.7 Gauss/cm) bipolar crusher gradient (filled circles). The solid line through the filled circles is the fit to Eq. [2] by using the average value of $R_1(\omega_1,\Delta\omega)$ determined for the gray matter ROI. Data from Subject 4.

Although Eq. [2] cannot be used to analyze data taken in the absence of bipolar crusher gradients, the apparent arterial transit time under these conditions can be estimated by extrapolating the data to $\Delta M/M_0 = 0$. The apparent arterial transit time measured in the absence of strong crusher gradients would be expected to reflect the time required for water to move from the tagging plane to small arteries in the imaging slice. For the data shown in the top of Fig. 5, the apparent arterial transit time in the absence of bipolar crusher gradients is ~0.5 s.

The experiment shown in Fig. 5 was performed three times on the same individual (on different days). The average value of τ_a was 0.93 ± 0.09 s, while the average
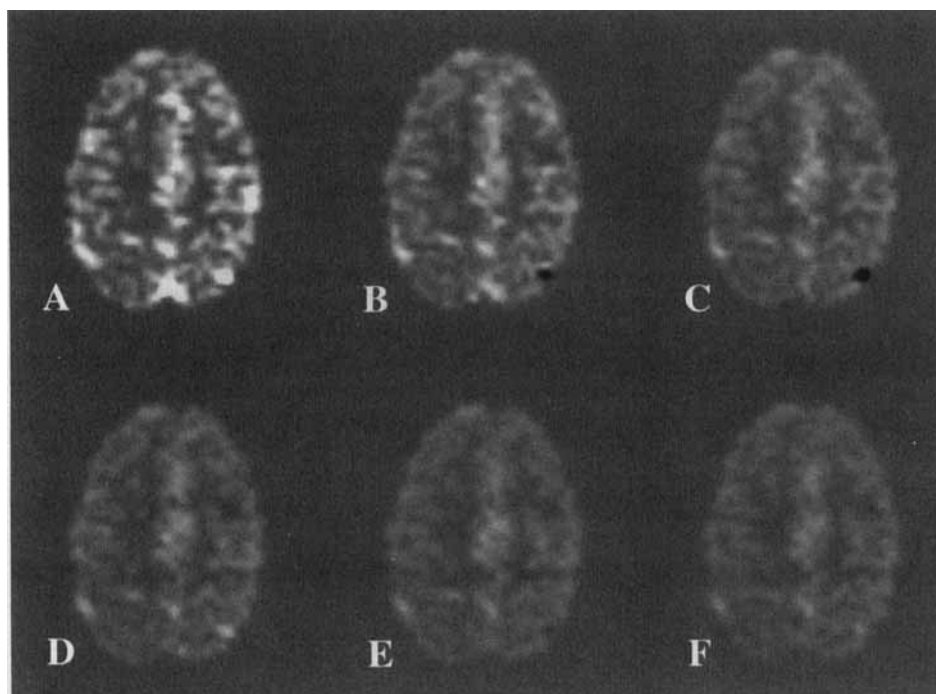

FIG. 4. Images of ΔM for the slice shown in Fig. 1. Images were calculated for six different values of the amplitude of the bipolar crusher gradient, G (Gauss/cm): (A) 0, (B) 0.24, (C) 0.48, (D) 0.96, (E) 1.43, (F) 1.7. The length of the off-resonance RF pulse train, τ_{RF}, was 3.6 s. Data from Subject 4.

value of $\Delta M/M_0$ was $0.53 \pm 0.05\%$. In the presence of the strong bipolar crusher gradients, the average value of $\Delta M(\tau_{RF})/M_0$ for the interval $0 \le \tau_{RF} < 0.6$ s was $0.01 \pm 0.03\%$ (mean $\pm$ SD, $N = 18$). In the absence of the bipolar crusher gradients, the average value of the apparent arterial transit time was ~0.5 s.

Figure 6 shows a set of data similar to that shown in Fig. 5, except the values of $\Delta M(\tau_{RF})/M_0$ were averaged over an ROI containing approximately 70 "arterial" voxels (see Materials and Methods section). An extrapolation of the data acquired in the absence of strong bipolar crusher gradients to $\Delta M/M_0 = 0$ gives a value of ~0.15 s. This value would be expected to reflect the time required for water to move from the tagging plane to large arteries in the imaging slice. The data taken in the presence of the strong bipolar gradients (bottom data set) suggest that the "arterial" voxels contained significant amounts of brain tissue.

Figure 7 shows a series of ΔM images taken at different values of τ_{RF} using two different values of the amplitude of the bipolar crusher gradient, i.e., 0 and 1.7 Gauss/cm. ΔM images acquired in the absence of the bipolar crusher gradients show bright foci that appear at short values of τ_{RF}, and remain at long values of τ_{RF}. These bright foci, which are absent from ΔM images taken in the presence of the bipolar crusher gradients, presumably arise from tagged water in large arteries.

Determination of τ_a and Q by Using a Modified Protocol

We assumed that the conclusions obtained with Subject 4, i.e., that the large bipolar gradients effectively crushed the signal from tagged arterial spins and that the dependence of ΔM on τ_{RF} could be described by a single-compartment model, could be extrapolated to all of the subjects (see Discussion section). We then analyzed the data for all of the subjects by using Eqs. [2]–[4].

The protocol illustrated in Fig. 5 was modified to reduce the total time for the examination, and to increase
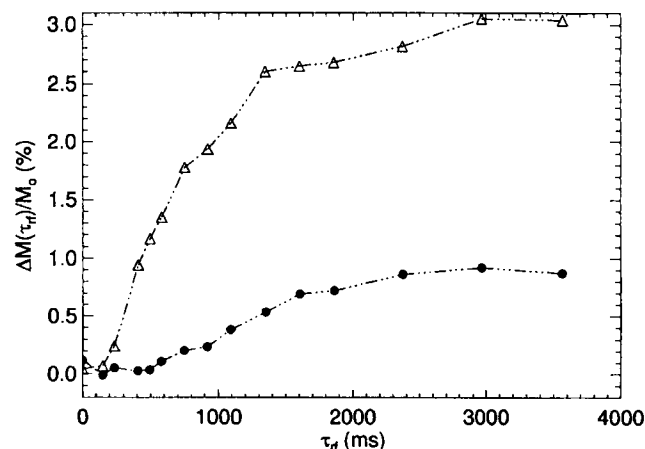

FIG. 6. Dependence of $\Delta M/M_0$ on the length of the off-resonance RF pulse train, τ_{RF}. $\Delta M/M_0$ values were averaged for an ROI containing approximately 70 "arterial" voxels (see Materials and Methods section). Data were taken in the absence of the bipolar crusher gradient (triangles) and in the presence of a large (1.7 Gauss/cm) bipolar crusher gradient (filled circles). Data from Subject 4.

the signal-to-noise ratio of the $\Delta M(\tau_{RF})/M_0$ image acquired with $\tau_{RF} = 3.6$ s (see Material and Methods section). First, no data was obtained in the absence of bipolar gradients, except for one value of τ_{RF} (3.6 s). This data point was used to exclude "arterial" voxels from the data analysis (see above) and to monitor the efficacy of the bipolar crusher gradients (see below). Second, no data was obtained for $\tau_{RF} < 0.7$ s, because the single-compartment model predicts that $\Delta M(\tau_{RF})/M_0 = 0$ for $\tau_{RF} \le \tau_a$. Third, the value of $\Delta M(\tau_{RF} = 3.6 \text{ s})/M_0$ was averaged for longer times (see Materials and Methods section).

A typical data set obtained by using the modified protocol is shown in Fig. 8, which shows the average value of $\Delta M/M_0$ for the gray matter ROI (see Materials and Methods section) as a function of τ_{RF}. For the data shown in Fig. 8, the calculated value of τ_a for the gray matter ROI was 0.71 s. Using this value for τ_a, the degree of water spin inversion in the capillaries, i.e., α_{cap}, was calculated by using Eq. [4], assuming that $T_{1a} = 1.2$ s (see below). The value of α_{cap} calculated from the data shown in Fig. 8 was 0.49.

We assumed that the value of α_{cap} for individual voxels was the same as the average value of α_{cap} determined for the gray matter ROI. This assumption was made for two reasons. First, the signal-to-noise ratio of the data was not sufficient to use the analysis outlined in Figs. 5 or 8 to calculate τ_a for individual voxels in the gray matter ROI. Second, the values of $\Delta M/M_0$ for white matter are too small to use the analysis outlined in Figs. 5 or 8 to calculate the average value of τ_a for the white matter ROI. Using the average value of α_{cap} for the gray matter ROI, the cerebral blood flow in each voxel was calculated from the observed value of $\Delta M/M_0$ at $\tau_{RF} = 3.6$ s by using Eq. [3], and the observed values of $R_1(\omega_1, \Delta\omega)$, assuming $\lambda = 0.90$ (18). The calculated cerebral blood flow image is shown in Fig. 9.

The protocol illustrated in Fig. 8 was performed on a total of seven normal volunteers (three females, four males, average age $= 35 \pm 9$). Average cerebral blood flow values for the gray matter ROI and the white matter ROI are shown in Table 1. Table 1 also shows the average blood flow values for a "whole brain" ROI, which included all the brain voxels in the image except those designated as "arterial" voxels or CSF voxels (see Materials and Methods section), and the values of τ_a for the gray matter ROI.

For the seven subjects the average reduction in $\Delta M/M_0$ for the gray matter ROI on application of the strong crusher gradients ($G = 1.7$ Gauss/cm, $\tau_{RF} = 3.6$ s) was $43 \pm 8\%$. This average reduction is similar to the reduction in $\Delta M/M_0$ found in the data shown in Fig. 3 for $G = 1.7$ Gauss/cm, i.e., ~49%.

Longitudinal Relaxation Time of Oxygenated Blood

The longitudinal relaxation time of oxygenated blood, measured at 63.9 MHz and 37°C, was 1.2 s (J. Vymazal and J. Bulte, personal communication). The accuracy of the measured relaxation time was estimated to be approximately $\pm 2\%$ (15).
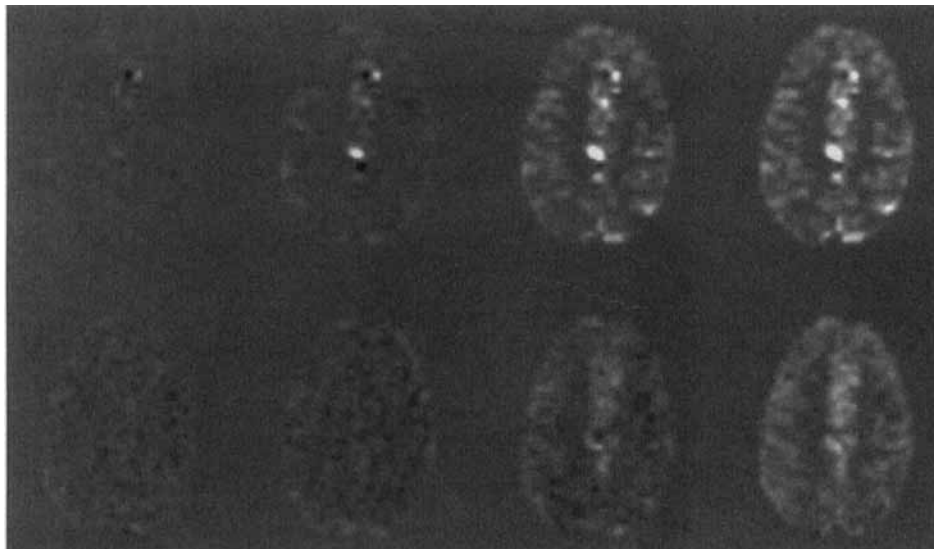
FIG. 7. Images of ΔM for the slice shown in Fig. 1. Images were calculated for four different values of τ_{RF}, and two different values of the amplitude of the bipolar crusher gradient, G. The top set of data was acquired with $G = 0$ Gauss/cm; the bottom set of data was acquired with 1.7 Gauss/cm. The values of τ_{RF} were (from left to right) 0.24 s, 0.40 s, 1.3 s, 3.0 s. Data from Subject 4.

DISCUSSION

Arterial spin tagging approaches have been used to image cerebral blood flow in animals (1–5) and humans (6–8). Several factors that affect the precision and accuracy of calculated cerebral blood flow values are the intrinsic signal-to-noise, the longitudinal relaxation times of water in arterial blood and brain tissue, the arterial transit time, and the magnitude of the cerebral blood flow (see Eqs. [3] and [4]). In studies with small animals at high magnetic field strengths, these factors are relatively favorable. However, in studies with humans at 1.5 T, these factors are all relatively unfavorable, and the precision and accuracy of cerebral blood flow values can be poor. The work presented here investigates two systematic errors that are important in human spin tagging experiments at 1.5 T.

The first systematic error involves the contribution from tagged water to the observed change in brain water magnetization. Tagged arterial water in large arteries gives rise to bright "foci" in ΔM images taken in the
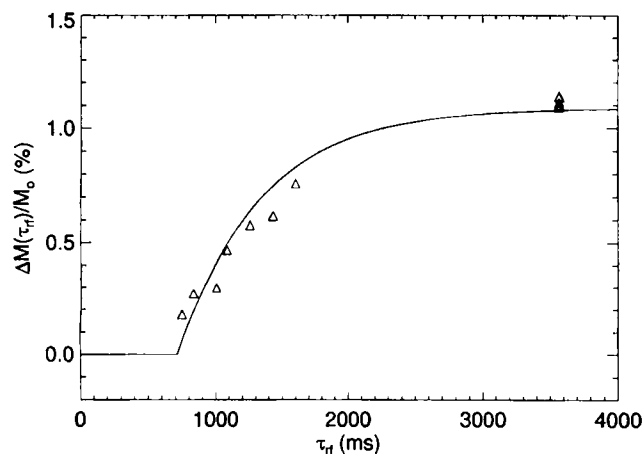

FIG. 8. Dependence of $\Delta M/M_0$ on the length of the off-resonance RF pulse train, τ_{RF}. $\Delta M/M_0$ values were averaged for all voxels in the gray matter ROI. The protocol was modified from the protocol shown in Fig. 5. Six data points were obtained for $\tau_{RF} = 3.6$ s. Data from Subject 6.

absence of strong bipolar crusher gradients (see Fig. 7). While tagged water in small arteries does not give rise to heterogeneous bright foci, it can contribute to the value of ΔM. In general, the volume of blood in small arteries is a small fraction of the total brain volume, i.e., ~1% (19). However, the perturbation in arterial water magnetization can be one to two orders of magnitude larger than the perturbation in intracellular water magnetization. Under these conditions, the contributions to ΔM from the arterial microvasculature and brain tissue can be comparable.

The contribution of arterial water spins to ΔM can be reduced if large crusher gradients are used to dephase the signal from moving spins (20–22). Figure 3 demonstrates that application of a large bipolar crusher gradient (1.7 Gauss/cm) reduced ΔM by approximately 49%. The small effect of the crusher gradients on M_{ss} (~3%) implies that the effects of the crusher gradients on ΔM are not simply due to diffusion of intracellular water through the applied field gradients (16). The simplest interpretation of these data is that in the absence of bipolar crusher gradients, ΔM arises almost equally from arterial water and intracellular water, whereas in the presence of large bipolar crusher gradients, ΔM arises predominantly from intracellular water.

The second systematic error involves longitudinal relaxation of tagged arterial water during transit from the tagging plane to capillary exchange sites in the imaging slice. Longitudinal relaxation reduces the degree of inversion of arterial water spins at the capillary exchange site, i.e., α_{cap}. If the arterial transit time, τ_a, is known, α_{cap} can be calculated by using Eq. [4]. Zhang et al. (23) developed a "dynamic" spin tagging approach that could be used to estimate τ_a, and showed that in the rat τ_a was much smaller than T_{1a}. In the rat, α_{cap} is therefore similar to α_0, the degree of inversion at the tagging plane. However, the data presented here demonstrate that in the human τ_a (~0.94 s) and T_{1a} (~1.2 s) are comparable, and α_{cap} is thus much smaller than α_0. A typical value of α_{cap}/α_0 for the data presented here was ~0.45.

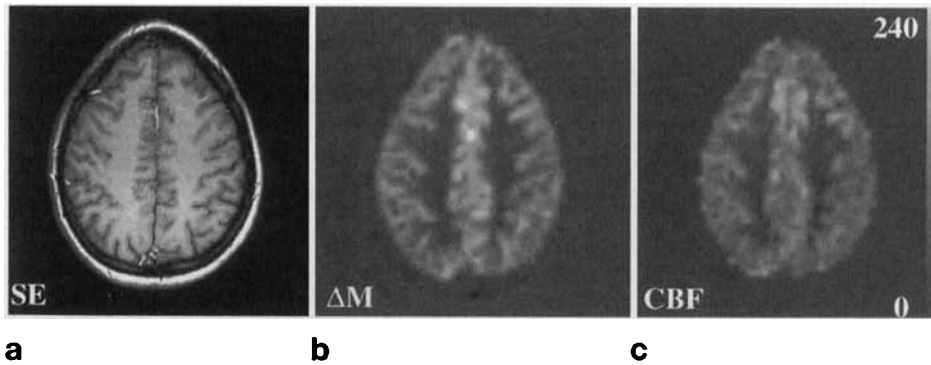The results discussed above demonstrate that arterial contributions to $\Delta M/M_0$ could result in an over-estima-

FIG. 9. Images of the slice shown in Fig. 1: (a) anatomical image (SE 500/20), (b) ΔM image taken in the presence of large (1.7 Gauss/cm) bipolar crusher gradients with $\tau_{RF} = 3.6$ s, (c) cerebral blood flow (cc/100 g/min) image. Data from Subject 6.

tion of Q by a factor of two, whereas relaxation of tagged water spins during arterial transit could result in an under-estimation of Q by a factor of two. Both "vascular" artifacts are thus important, but tend to cancel each other.

The quantitative determination of human cerebral blood flow values by using arterial spin tagging approaches requires correction for both "vascular" artifacts. In the work presented here, we performed extensive studies on one subject (No. 4) to verifiy that the the bipolar crusher gradient was effective in crushing signal from tagged arterial blood, and that the dependence of ΔM on τ_{RF} could be described by a single-compartment model (see Figs. 3 and 5). However, because of the long examination times (see Materials and Methods section), it was not practical to repeat the complete protocols illustrated in Figs. 3 and 5 on all of the subjects. We therefore assumed that the conclusions obtained for Subject 4 could be applied to all of the subjects. This assumption is consistent with a number of ancillary observations. First, the experiment shown in Fig. 3 was repeated once on another subject (No. 7), with similar results. Second, for $G = 1.7$ Gauss/cm and $\tau_{RF} = 3.6$ s, the average reduction in $\Delta M/M_0$ for all of the subjects, i.e., $43 \pm 8\%$, is similar to the decrease observed in Fig. 3 under these conditions, i.e., $\sim 49\%$. Third, by using the modified protocol, the data sets observed for all of the subjects were consistent with the single-compartment model, e.g., see Fig. 8. Fourth, the average value of τ_a for all the subjects (0.94 ± 0.14 s), calculated by using the modified protocol, is similar to the average value of τ_a, calculated for Subject 4 (0.93 ± 0.09 s) by using the protocol outlined in Fig. 5.

The methods used to correct for vascular artifacts substantially decrease the signal-to-noise of the measured $\Delta M/M_0$ values, and substantially lengthen the examination time. For example, in the protocol illustrated in Fig. 8, approximately one third of the total examination time was used to measure τ_a. One way to circumvent these constraints could be to use ΔM images (see Fig. 9) as a qualitative measure of perfusion. Another way to circumvent these constraints is to optimize the signal-to-noise of the spin tagging experiment. One way to increase the signal-to-noise of the $\Delta M/M_0$ images could be to use higher magnetic field strengths, where the intrinsic signal-to-noise ratio may be higher, and the longitudinal relaxation times may be longer. Another way is to reduce the magnetization transfer effects of the off-resonance RF irradiation, which can be done by using a "two-coil" system (7, 24).

Mean cerebral blood flow values for the gray matter ROI and white matter ROI (see Table 1) are in reasonable agreement with gray matter and white matter blood flow values determined in the human brain by using ^{15}O PET approaches (25). The mean cerebral blood flow value for the "whole brain" ROI (61 ± 15 cc/100 g/min) is slightly higher, but in reasonable agreement with, mean whole brain cerebral blood flow values determined by using the Kety-Schmidt approach, i.e., ~ 55 cc/100 g/min (26).

Cerebral blood flow values calculated by using the procedures outlined above to correct for vascular artifacts are still subject to a number of systematic errors. First, failure of the bipolar gradients to crush completely signals from tagged arterial water spins could lead to an over-estimation of the true cerebral blood flow. Second, variation of τ_a among gray or white matter voxels, or

Table 1
Cerebral Blood Flow Values for Seven Normal Subjects

Subject	Sex	Age (years)	τ_a (s)	Q_{gray} (cc/100 g/min)	Q_{white} (cc/100 g/min)	Q_{brain} (cc/100 g/min)
1	M	28	0.96	75	25	57
2	M	30	1.16	74	15	54
3	M	32	1.05	80	13	56
4	M	50	0.91	47	26	40
5	F	25	0.91	109	35	88
6	F	35	0.71	101	24	73
7	F	42	0.90	79	24	60
			0.94 ± 0.14	81 ± 20	23 ± 7	61 ± 15

Cerebral blood flow values were obtained from the slice represented in Fig. 1. Q_{gray} and Q_{white} are average cerebral blood flow values for the gray and white matter ROI (see Materials and Methods section). Q_{brain} is the average cerebral blood flow value for all brain voxels in the slice, except those designated as "arterial" voxels or "CSF" voxels (see Material and Methods section).

partial volume effects in the calculation of longitudinal relaxation rates and $\Delta M/M_0$ values, could lead to an underestimation or overestimation of the true cerebral blood flow value. Other systematic errors that have been discussed previously involve asymmetric magnetization transfer effects and gradient eddy current effects (5, 27). However, the observation that $\Delta M/M_0$ is not significantly different from zero for $\tau_{RF} < \tau_a$ (see Fig. 5 and Results section) suggests that the four-step protocol used here provides adequate correction for asymmetric magnetization transfer effects and gradient eddy current effects.

The vascular artifacts discussed here may be substantially larger, and more difficult to correct, in patients with regional perfusion deficits. For example, the large value of τ_a in infarcted brain regions could significantly reduce the value of α_{cap} in that region, according to Eq. [4].

Analysis of the dependence of $\Delta M/M_0$ on τ_{RF} under different conditions allows an estimate of three different arterial transit times. The shortest transit time (~ 0.15 s) was observed for an ROI composed of "arterial" voxels in the absence of bipolar crusher gradients (see Fig. 6). This transit time presumably reflects the time for water to move from the tagging plane to large arteries in the imaging slice. The average blood velocity estimated by using the transit time was $\leqslant 20$ cm/s. The second in the series of three transit times (~ 0.5 s) was observed for the gray matter ROI in the absence of bipolar crusher gradients (see top curve, Fig. 5). This transit time presumably reflects the time for water to move from the tagging plane to small arteries in the imaging slice. In spite of differences in experimental approaches, the transit time reported here for the gray matter ROI in the absence of large bipolar crusher gradients was similar to the transit time observed by Buxton et al. (28) for a gray matter ROI in the absence of crusher gradients (~ 0.5 s). The longest transit time (~ 0.94 s) was observed for the gray matter ROI in the presence of large bipolar crusher gradients (see bottom curve, Fig. 5). This transit time, defined above as τ_a, presumably reflects the time for water to move from the tagging plane to capillary exchange sites in the imaging slice. It should be noted that the model used to define τ_a (see Appendix) assumes that water is a "diffusible" tracer. If this is not the case, τ_a can still be defined operationally by Eq. [2].

The differences observed among the three transit times discussed above suggest that there is a substantial delay (~ 0.4 s) between the arrival of tagged blood in small arteries in the imaging slice and the arrival of tagged blood at capillary exchange sites in the imaging slice, and also suggest that a large fraction of the time required for water to move from the tagging plane to capillary exchange sites in the imaging slice involves redistribution of blood within the arterial microcirculation in the imaging slice. A corollary would be that, even if the tagging plane were moved to the proximal boundary of the imaging slice, water would still require ~ 0.5 s to move from the tagging plane to capillary exchange sites in the imaging slice.

In summary, "vascular" artifacts can cause substantial errors in human cerebral blood flow values calculated by using spin tagging approaches at 1.5 T. The work presented here suggests several procedures that can reduce, or correct for, these artifacts. Cerebral blood flow values calculated for normal volunteers by using these procedures agree reasonably well with values calculated by using radioactive tracer approaches.

APPENDIX

The effects of magnetization transfer from macromolecular protons to water protons in the presence of off-resonance RF irradiation can be interpreted in terms of a simple four-compartment model (11). We assume that the concentration of macromolecular protons in brain tissue is much less than the concentration of water protons, that the exchange of water molecules from sites that give magnetization transfer between bound water protons and macromolecular protons is in the "fast-exchange" limit in the absence of off-resonance RF irradiation, and that the observed longitudinal relaxation time of water protons is much longer than the transverse relaxation times of water protons or macromolecular protons. Under these conditions, the longitudinal magnetization of bulk water protons, $M(t)$, can be shown to obey the simple differential equation

$$\frac{dM(t)}{dt} = -R_1(\omega_1, \Delta\omega)\{M(t) - M_{ss}(\alpha, \omega_1, \Delta\omega)\} \quad [A1]$$

where $R_1(\omega_1, \Delta\omega)$ and $M_{ss}(\alpha, \omega_1, \Delta\omega)$ are the longitudinal relaxation rate, and the steady state longitudinal magnetization, of bulk water protons in the presence of off-resonance RF irradiation (11). Equation [A1] assumes that $R_1(\omega_1, \Delta\omega)$ and α are constant.

Equation [A1] is similar to the differential equation derived by using projection operator approaches, i.e, Eq. [10] of Adler and Yeung (29). In fact, for $\alpha = 0$, Eq. [A1] can be shown to be equivalent to Eq. [10] of Adler and Yeung (29) if approximations corresponding to those used here are invoked.

The general solution to Eq. [A1] is

$$M(t) = M(0)e^{-\int_0^t R_1(\omega_1, \Delta\omega)d\tau'}$$

$$[A2]$$

$$+ \int_0^t e^{-\int_\tau^t R_1(\omega_1, \Delta\omega)d\tau'} R_1(\omega_1, \Delta\omega)M_{ss}(\alpha, \omega_1, \Delta\omega)d\tau$$

Equation [A2] is also valid if $R_1(\omega_1, \Delta\omega)$ and α are "piecewise" constant over the interval 0 to t, i.e., if $R_1(\omega_1, \Delta\omega)$ and α are constant in each of a finite number of subintervals between 0 and t, but not the same from one subinterval to the next.

We define the normalized difference between the amplitude of the signals obtained from the "tagging" scan and the "control" scan as $\Delta M/M_0$, i.e.,

$$\frac{\Delta M(t)}{M_0} \equiv \frac{M(\alpha, t) - M(\alpha = 0, t)}{M_0} \quad [A3]$$

If the control scan is performed under the same conditions as the "tagging" scan, except that $\alpha = 0$, the expres-

sion for $\Delta M(t)M_0$ given by Eq. [A2] is

$$\Delta M(t)/M_0 = -2\,Q/\lambda \int_0^t e^{-\int_\tau^t R_1(\omega_1,\Delta\omega)d\tau'}\,\alpha(t)d\tau \quad [A4]$$

where we have used the relationship (11)

$$R_1(\omega_1,\Delta\omega)\{M_{ss}(\alpha,\omega_1,\Delta\omega) - M_{ss}(\alpha = 0,\,\omega_1,\Delta\omega)\}$$
$$= -2\,\alpha\,Q/\lambda\,M_0 \quad [A5]$$

We assume that the time dependence of $\alpha(\tau)$ is given by

$$\alpha(\tau) = 0 \quad \text{for} \quad 0 \leq \tau \leq \tau_a$$
$$\alpha(\tau) = \alpha_{cap} \quad \text{for} \quad \tau_a < \tau$$

where τ_a is the arterial "transit time," i.e, the time required for tagged blood to move from the tagging plane to capillary exchange sites in the imaging slice, and α_{cap} is the value of α in the capillary. Eq. [A4] then becomes

$$\Delta M(t)/M_0 = \frac{-2\,\alpha_{cap}\,Q/\lambda}{R_1(\omega_1,\Delta\omega)}\{1 - e^{-R_1(\omega_1,\Delta\omega)(t-\tau_a)}\} \quad [A6]$$

where $R_1(\omega_1,\Delta\omega)$ is the water relaxation rate in the presence of the off-resonance RF irradiation used for tagging. The use of Eq. [A6] to interpret the time dependence of $\Delta M(t)/M_0$ assumes that the tagging and the control scans have the same value of $M(0)$ (see Eq. [A2]). The tagging and the control scans will have the same value of $M(0)$ if the delay between the scans is much larger than the longitudinal relaxation time. However, by using a spin-echo EPI sequence with a 90° pulse, the tagging and the control scan will have the same value of $M(0)$ regardless of the repetition rate.

The use of Eq. [A6] to interpret the time dependence of $\Delta M(t)/M_0$ is complicated by the fact that tagged arterial water spins located between the tagging plane and the imaging slice will continue to enter the imaging slice when the tagging is turned off. However, if data for the four-pulse sequence are taken in the order (control, tag, tag, control), subtraction of the control data from the tagging data compensates for the delayed entry of tagged arterial blood into the imaging slice.

ACKNOWLEDGMENTS

REFERENCES

1. J. A. Detre, J. S. Leigh, D. S. Williams, A. P. Koretsky, Perfusion Imaging. *Magn. Reson. Med.* **23**, 37–45 (1992).

2. D. S. Williams, J. A. Detre, J. S. Leigh, A. P. Koretsky, Magnetic resonance imaging of perfusion using spin inversion of arterial water. *Proc. Natl. Acad. Sci. USA* **89**, 212–216 (1992).

3. E. G. Walsh, K. Minematsu, J. Leppo, S. C. Moore, Radioactive microsphere validation of a volume localized continuous saturation perfusion measurement. *Magn. Reson. Med.* **31**, 147–153 (1994).

4. J. R. Ewing, J. M. Boska, Y. Cao, S. Brown, Z. G. Zhang, K. M. A. Welch, A fast method for measuring cerebral perfusion using arterial spin labeling and variable flip-angle FLASH imaging, *in* "Proc., SMR, 3rd Annual Meeting," Nice, France, 1995," p. 871.

5. J. Pekar, P. Jezzard, D. A. Roberts, J. S. Leigh, J. A. Frank, A. C.

McLaughlin, Perfusion Imaging with compensation for asymmetric magnetization transfer effects. *Magn. Reson. Med.* **35**, 70–79 (1996).

6. D. A. Roberts, J. A. Detre, L. Bolinger, E. K. Insko, J. S. Leigh, Quantitative magnetic resonance imaging of human brain perfusion at 1.5 T using steady-state inversion of arterial water. *Proc. Natl. Acad. Sci. USA* **91**, 33–37 (1994).

7. J. A. Detre, W. Zhang, D. A. Roberts, A. C. Silva, D. S. Williams, D. J. Grandis, A. P Koretsky, J. S. Leigh, Tissue specific perfusion imaging using arterial spin labeling. *NMR Biomed.* **7**, 75–82 (1994).

8. F. Q. Ye, J. J. Pekar, P. Jezzard, J. Duyn, J. A. Frank, A. C. McLaughlin, Perfusion imaging of the human brain at 1.5 T using a single-shot EPI spin tagging approach. *Magn. Reson. Med.* **36**, 219–224 (1996).

9. W. T. Dixon, L. N. Du, D. D. Faul, M. Gado, S. Rossnick, Projection angiograms of blood labelled by adiabatic fast passage. *Magn. Reson. Med.* **3**, 454–462 (1986).

10. P. R. Bevington, "Data Reduction and Error Analysis for the Physical Sciences," pp. 235–240, McGraw-Hill, New York, 1969.

11. A. C. McLaughlin, F. Q. Ye, J. Pekar, A. K. S. Santha, J. A. Frank, Effect of magnetization transfer on the measurement of cerebral blood flow using steady-state arterial spin tagging approaches: a theoretical investigation. *Magn. Reson. Med.* (in press).

12. R. B. Balaban, T. L. Ceckler, Magnetization transfer contrast in magnetic resonance imaging. *Magn. Reson. Q.* **8**, 116–137 (1992).

13. J. C. Rajapakse, J. N. Giedd, C. DeCarli, J. W. Snell, A. C. McLaughlin, Y. C. Vauss, A. L. Krain, S. Hamburger, J. L. Rapoport, A technique for single-channel MR brain tissue segmentation: application to a pediatric sample. *Magn. Reson. Imaging*, in press.

14. R. A. Brooks, J. Vymazal, J. W. M. Bulte, C. D. Baumgarner, V. Tran, Comparison of T2 relaxation in blood, brain, and ferritin. *J. Magn. Reson. Imaging* **4**, 446–450 (1995).

15. J. Vymazal, O. Zak, J. W. M Bulte, P. Aisen, R. A. Brooks, T_1 and T_2 of Ferritin Solutions: effect of loading factor. *Magn. Reson. Med.* **36**, 61–65 (1996).

16. D. Le Bihan, R. Turner, Diffusion and perfusion, *in* "Magnetic Resonance Imaging" (D. D. Stark, W. G. Bradley, Jr, Eds.), pp. 355–371, 2nd Ed., Mosby, St. Louis, 1992.

17. G. E. Medical Systems, "Vascular Magnetic Resonance Imaging, Volume III," pp. 29, G. E. Medical Systems, Milwaukee, 1990.

18. P. Herscovitch, M. E. Raichle, What is the correct value for the brain-blood partition coefficient for water? *J. Cereb. Blood Flow Metab.* **5**, 65–69 (1985).

19. M. A. Mintun, M. E. Raichle, W. R. W. Martin, P. Herscovitch, Brain oxygen utilization measured with O-15 radiotracers and positron emission tomography. *J. Nucl. Med.* **25**, 177–187 (1984).

20. J. L. Boxerman, P. A. Bandettini, K. K. Kwong, J. R. Baker, T. L. Davis, B. R. Rosen, R. M. Weisskoff, The intravascular contribution to fMRI signal change: Monte Carlo modeling and diffusion-weighted studies *in vivo. Magn. Reson. Med.* **34**, 4–10 (1995).

21. A. W. Song, E. C. Wong, S. G. Tan, J. S. Hyde, Diffusion weighted fMRI at 1.5 T. *Magn. Reson. Med.* **35**, 155–158 (1996).

22. R. S. Menon, X. Hu, G. Adriany, P. Anderson, S. Ogawa, K. Ugurbil, Comparison of spin-echo EPI, asymmetric spin-echo EPI and conventional EPI applied to functional neuroimaging: the effect of flow crushing gradients on the BOLD signal, *in* "Proc., SMR, 2nd Annual Meeting," San Francisco, 1994," p. 622.

23. W. Zhang, D. S. Williams, J. A. Detre, A. P. Koretsky, Measurement of brain perfusion by volume-localized NMR spectroscopy using inversion of arterial water spins: accounting for transit time and cross-relaxation. *Magn. Reson. Med.* **25**, 362–371 (1992).

24. W. Zhang, A. C. Silva, D. S. Williams, A. P. Koretsky, NMR measurement of perfusion using arterial spin labeling without saturation of macromolecule spins. *Magn. Reson. Med.* **33**, 370–376 (1995).

25. R. S. J. Frackowiak, G-L. Lenzi, T. Jones, J. D. Heather, Quantitative measurement of regional cerebral blood flow and oxygen metabolism in man using 15O and positron emission tomography: theory, procedure, and normal values. *J. Comput. Asst. Tomogr.* **4**, 727–736 (1980).

26. B. K. Siesjo, "Brain Energy Metabolism," p. 74, John Wiley, New York, 1978.

27. A. D. Stein, D. A. Roberts, J. McGowan, R. Reddy, J. S. Leigh, Asymmetric cancellation of magnetization transfer effects, *in* "Proc., SMR, 2nd Annual Meeting, San Francisco, 1994," p. 880.

28. R. B. Buxton, L. R. Frank, B. Siewert, S. Warach, R. R. Edelman, A quantitative model for EPISTAR perfusion imaging, *in* "Proc., SMR, 3rd Annual Meeting," Nice, France, 1995," p. 132.

29. R. S. Adler, H. N. Yeung, Transient decay of longitudinal magnetization in heterogeneous spin systems under selective saturation. III. Solution by projection operators. *J. Magn. Reson. Series A* **104**, 321–330 (1993).